Materials Sciences and Applications, 2025, 16(1), 27-45
https://www.scirp.org/journal/msa
ISSN Online: 2153-1188
ISSN Print: 2153-117X

Reactive Oxygen Species (ROS) Generated on the Surface of (100)-Plane Grain-Oriented Copper Thin-Film

Ken Hirota[1*], Taika Maeda[2], Kazuhiko Tsukagoshi[2], Yurika Taniguchi[3], Hiroshi Kawakami[3], Takashi Ozawa[4], Masahiko Wada[4]

[1]Research Center of Bio-Micro-Fluidic Science, Doshisha University, Kyoto, Japan
[2]Department of Chemical Engineering and Materials Science, Faculty of Science & Engineering, Doshisha University, Kyoto, Japan
[3]Graduate School of Engineering, Osaka Metropolitan University, Osaka, Japan
[4]Japan Copper Development Association, Tokyo, Japan
Email: *khirota@mail.doshisha.ac.jp

How to cite this paper: Hirota, K., Maeda, T., Tsukagoshi, K., Taniguchi, Y., Kawakami, H., Ozawa, T. and Wada, M. (2025) Reactive Oxygen Species (ROS) Generated on the Surface of (100)-Plane Grain-Oriented Copper Thin-Film. *Materials Sciences and Applications*, **16**, 27-45.
https://doi.org/10.4236/msa.2025.161003

Received: December 9, 2024
Accepted: January 23, 2025
Published: January 26, 2025

Abstract

This work aims to study the dependence of the antibacterial activity on the crystal plane of Cu. The generation of reactive oxygen species (ROS) on the thin film of Cu with grains oriented in the plane (100) was evaluated by chemiluminescence (CL). The authors proposed the generation mechanism of these three ROS on the outermost surface consisting of Cu_2O thin film, CuO layer and bulk Cu.

Keywords

Copper, Crystal Planes, Antibacterial Activity, Reactive Oxygen Species, Chemiluminescence

1. Introduction

As already reported [1], copper (Cu) and its alloys, such as brass (Cu-Zn) and bronze (Cu-Sn), have been widely recognized as antibacterial materials [2], and they have been utilized as such as a drinking water vessel, the parts of religious buildings or a balustrade of bridge. However, these usages are, in general, performed with polycrystal Cu and alloys even in high purity due to the very expensive price of single crystal, few reports are available concerning about the dependence of antibacterial activity on the crystal plane of Cu. Up to now, antibacterial activity of Cu [3] [4] has been explained mainly by the reactive oxygen species (ROS) [5] generated on the metal surfaces, on which thin copper oxide layers, such as Cu_2O and CuO, are formed in air: at first, Cu_2O is formed on the surface of Cu under

moderate atmosphere and then CuO is formed on the Cu_2O layer [6]. Therefore, it is important to control the properties of these double layers of Cu_2O/CuO, such as each thickness, shape, continuous or "island" thin-films, and chemical/physical activity (stability), because ROS might be generated near this layer based on "Fenton reaction" [1] [7] as widely circulated.

In general, the formation of metal oxide thin-film depends on the crystal plane of substrate, for example, the epitaxial growth [8] of silicon oxide film [9] on the single-crystal silicon is well-known and studied because of its wide semiconductive applications [10]. Then, we thought that it was useful information if the relationship between antibacterial activity and the crystal plane of Cu could be clear. However, as mentioned above, it is difficult to use the very expensive single crystal, then we have focused on the crystal-plane (100) grain-oriented Cu thin-film, which has been recently developed [11] by "JX" Advanced Metals Corporation, Tokyo, Japan. We thought that this film would show the same behavior as the single crystal, as will be described and speculated in 3.3 later, *i.e.* the dependence of antibacterial activity on the Cu crystal-plane (100).

The purpose of this study is to inquire which crystal plane of Cu is superior to the production of ROS (*i.e.* resulting in high antibacterial activity), the crystal plane dependence on the chemiluminescence (CL) intensity for the grain-oriented Cu thin-films was investigated. It was clear that (100) plane could produce a higher CL intensity than those of (110) and (111) planes and in addition to this, the CL intensity depended much on the heat treatment for preparation of grain-oriented thin film, vacuum heating and followed re-oxidation conditions. 473 K for 1.8×10^3 s under vacuum and 373 K (4.2×10^2 s) or 398 K (1.8×10^3 s) in air, "re-oxidation", gave the around 10 times higher ΣCL (9 min) than that of as-obtained. In order to evaluate the outermost surface of thin-films, SEM and TEM observations have been performed. Furthermore, biotest using *Escherichia coli*, *Staphylococcus aureus,* and *A*/*Hong Kong virus* also has been performed in both long and short lapse times.

2. Experimental Procedure

2.1. Starting Materials

Starting materials were three kinds of Cu thin-films (JX Advanced Metals Corporation), name of commodity, HA, HA-V2 and TPC, with the style of roll packing (0.8 m width and 5 m long). Their futures supplied form "JX" were: 1) a thickness of 18 μm, 2) the grains on the flat surface would be highly oriented, *i.e.* a crystal plane of (100) would be dominant after the heat treatment of 473 K for 1.8×10^3 s (30 min) in an inert atmosphere. Their (100) plane orientation degree Q (100) is the highest for HA, and decreased a little for HA-V2, and TPC. In the present study, a square shape in size 25×25 mm^2 was cut from the roll and used. These cut thin-films, after wiping their surfaces with ethanol, were heated under various atmosphere, such as N_2 (purity 99.9%) gas flow (100 mL/min) in the cylindrical electric furnace (the inside diameter of 60 mm) up to 473 K for 1.8×10^3 s, under conventional vacuum using the combined rotary and diffusion pumps (a degree

of vacuum: 1 - 3 × 10^{-3} Pa) with a rotary & diffusion pumps, and in air at 373 to 523 K for 4.2 × 10^{2} - 1.8 × 10^{3} s. The heat treatment in air was performed in quick heating and cooling.

2.2. Evaluation

2.2.1. Physicochemical Properties

Powder X-ray diffraction (XRD: Smartlab, Rigaku, Tokyo, Japan) analysis with Cu*Kα* radiation (a wavelength of 0.15418 nm) was utilized for identification of the crystalline phases and evaluation of both crystallite sizes and grain orientation Q(HKL) for crystal plane (HKL) using the following equation; Q(HKL) = [Σ*I*(HKL)/Σ*I*(HKL)] × 100(%). Here, Σ*I*(HKL) means the summation of (HKL) plane's diffraction intensity *I*(HKL), and Σ*I*(HKL) the summation of all (HKL) plane's diffraction intensities *I*(HKL). However, as the crystal structure of metal Cu is face-centered cubic (FCC) and due to the extinction law, Σ*I*(HKL) = *I*(200) and Σ*I*(HKL) = *I*(111) + *I*(200) + *I*(220) + *I*(311). The measuring conditions for powder XRD were as follows: accelerating electric voltage and current were 45 kV and 200 mA, respectively, scanning speed 1.667 × 10^{-1}˚/s (10˚/min), scanning angle 2*θ*: 40˚ - 100˚.

Microstructural observation with a field emission-type scanning electron microscope (FE-SEM; SU8020, Hitachi High-Technologies Corporation, Tokyo, Japan) and a transmission electron microscope (TEM, JEM-2100F, JEOL, Tokyo, Japan) equipped with the energy-dispersive X-ray spectroscopy (EDS, JED-2300T, JEOL) were performed. Before TEM observation, the Cu samples were cut into a small specimen using a focused ion beam (FIB, FB2200, Hitachi High-Technologies Corporation).

2.2.2. Chemiluminescence (CL) Intensity Measurement and Evaluation of Reactive Oxygen Species (ROS) [12]-[15]

Chemiluminescence (CL) of Cu thin-films [sample size of 2.5 × 10^{-3} m (25 mm) square] in a 2.5 × 10^{-7} m^3 (0.25 mL) aqueous luminol (Reagent special grade: purity > 95.0%) solution with a concentration of 5.0 × 10^{-1} - 5.0 × 10^{-2} mol·m^{-3} (5.0 × 10^{-4} - 5.0 × 10^{-5} mol·L^{-1}) mixed with 5.0 × 10^{-6} m^3 (5.0 mL) carbonic acid buffer solution ($NaOH/NaHCO_3$, pH = 10.7 - 10.9) [16] was observed under dark conditions K using a CL detector (CLA-FS3, Tohoku Electronic Industrial Co., Ltd., Sendai, Japan), during measurement temperature was kept at 293 by cooling/warming system to keep a constant temperature. After dropping the luminol solution in a 6.0 × 10^{1} s' warming up of the detector, the intensity of CL was integrated between 6.1 × 10^{1} and 6.0 × 10^{2} s (9 min) [14]. The obtained summation of CL intensity for 5.4 × 10^{2} s (9 min), ΣCL (9 min), which was calculated as follows: at first, estimate the summation of background noise, ΣCL (BG), from 0 to 6.0 × 10^{1} s, and then summarize the CL intensity from 6.1 × 10^{1} to 6.0 × 10^{2} s, ΣCL (total 9 min), finally, true ΣCL (9 min) was determined to be as the true ΣCL (9 min) = ΣCL (total 9 min) – ΣCL (BG) × 9. This true ΣCL (9 min), in a simple term, ΣCL (9 min) value was utilized to evaluate the amount of ROS generated from the surface of Cu thin-films.

Among 4 kinds of ROS, such as ·OH, H_2O_2, $\cdot O_2^-\cdot$ and $^1O_2$, scavengers [17] [18], 2-propanol [19] [20] ("2-pro", for ·OH, Nacalai Tesque Chemicals, Kyoto, Japan) [15]-[17], sodium pyruvate [19] ("s-pyr", for H_2O_2, Fuji-film Wako Pure Chemical Co., Ltd., Osaka, Japan), nitro blue tetrazolium [21] ("nbt", for $\cdot O^{2-}\cdot$, Nacalai Tesque Chemicals) and sodium azide [18] (for short "NaN_3", for $^1O_2$, Fuji-film Wako Pure Chemical) were mainly used to determine which ROS was generated. At first, these scavengers were solved into the buffer solution with the concentration 5.0×10^{-2} mol·m^{-3} (5.0×10^{-5} mol·L^{-1}) and then obtained 5.0×10^{-7} m^{-3} (0.50 mL) or 1.0×10^{-6} m^{-3} (1.0 mL) scavenger solution were used. Each solution and a 4.0×10^{-6} m^{-3} (4.0 mL) pure buffer solution were mixed. CL measurement was performed as the same as CL intensity measurement, after a 6.0×10^1 s' warming up of the detector, the intensity of CL was integrated between 6.0×10^1 - 6.0×10^2 s. The amount of difference (Δ) for each ROS was evaluated using the equation of

$$\Delta = \Sigma CL \text{ (9 min, without scavenger)} - \Sigma CL \text{ (9 min, with scavenger)} \quad (1)$$

2.2.3. Biotest of Cu Thin Films

As will be stated, two kinds of Cu thin films, *i.e.* 1) as-obtained HA thin film and 2) antibacterial activity improved HA film which was heated under vacuum (2.0×10^{-3} Pa) at 473 K for 1.8×10^3 s (30 min), followed by re-oxidation at 398 K for 4.2×10^2 s (30 min) in air were provided to biotest using *Escherichia coli* NBRC3301, *Staphylococcus aureus* NBRC 12732, and *A*/*Hong Kong*/8/68; TC adapted virus ATCC VR-1689 based on JIS (Japanese Industrial Standards) Z 2801 (Film adhesion method) by QTEC Technology Co., Ltd., Kobe City, Japan. These bacteria and viruses were adopted as follows: *Escherichia coli* was selected as a representative Gram-negative bacterium, *Staphylococcus aureus* as a representative Gram-positive bacterium, and *A*/*Hong Kong*/8/68; TC as a representative virus. Test conditions were as follows: The sample size was a square with 40×40 mm^2, *E. coli* 4.5×10^5 CFU/mL, *Staphylococcus aureus* 4.0×10^5 CFU/mL and *A*/*Hong Kong virus* 2.2×10^7 PFU/mL, and a PE film was used as a control. Biotest for two bacterial species and one virus was performed for 8.64×10^4 s (24 h) under dark condition. Furthermore, a short test of both as-obtained HA and antibacterial activity improved HA films using *E. coli* NBRC 3972 at 300 K for 1.8×10^3 s (30 min) in shade. Antibacterial activity value *R* was calculated by the following equation:

$$R = (\text{Log [control 30]-Log [control 0]}) - (\text{Log [sample 30]-Log [sample 0]})$$

3. Results and Discussion

3.1. (100)-Crystal-Plane Orientation Q(100) and Crystallite Sizes of Heated Cu Thin-Films

As described in experimental procedures 2.1 and 2.2.1, the as-obtained Cu thin-films, HA, HA-V2, and TPC, were heated in a N_2 gas flow. **Figure 1** shows powder XRD patterns of Cu thin-films (A) the as-obtained and (B) after the vacuum heating, respectively. In (A), all diffraction peaks such as (111), (200), (220), and (311) were confirmed, however, in (B), only (200) peak was recognized, indicating almost all grains were oriented to (200) plane, that is (100)-orientation (due to the

extinction rule for FCC, (100) diffraction peak cannot be observed). Then, all thin-films were heated at 373, 423, 473 and 523 K in N_2 and by their powder XRD measurement, Q(100) was evaluated. **Figure 2** shows their Q(100) values as a function of heating temperatures, with the Q(100) values of as-obtained conventional Cu plates ($25 \times 25 \times 1.0 \times 10^{-9}$ m^3) [1] and 473 K-heated as a reference. Q(100) of HA and HA-V2 started from 10.0/6.5% at 300 K (as-obtained) and increased rapidly to 99.8/96.2% at 423 K, finally saturated to 100/98.8% at 473 K, respectively. However, TPC increased Q(100) from 43.7% to 98.7% at 423 K, on the contrary, conventional Cu plate revealed 85.3% even at 473 K. Afterward, both HA and TPC films were focused on evaluation. To investigate the microstructural difference in crystallite size X_s at each crystal plane, which was determined by Scherrer's equation [22] ($X_s = K{\cdot}\lambda/(\beta{\cdot}\cos\theta$, here K: constant 1.0, λ: wave length 0.15418 nm, β: full width at half maximum, θ: diffraction angle) were estimated. **Figures 3-5** reveal X_s of as-obtained films, heated HA and TPC under various conditions, respectively. From **Figure 3**, it is worth noting that only X_s of (220) for as-obtained HA is very small at 16.3 nm, under that almost all X_s are 35 - 50 nm except for X_s of (311) are 30 nm. It should be noted that after various heat treatments (the precise conditions will be described later), HA showed a very large X_s of (200) about 160 nm, suggesting high Q(100) orientation (**Figure 4**). On the other hand, as shown in **Figure 5**, all X_s of TPC were the same from 100 to 120 nm except for (222) plane after heating. This behavior is thought to be common phenomena observed for conventional metals.

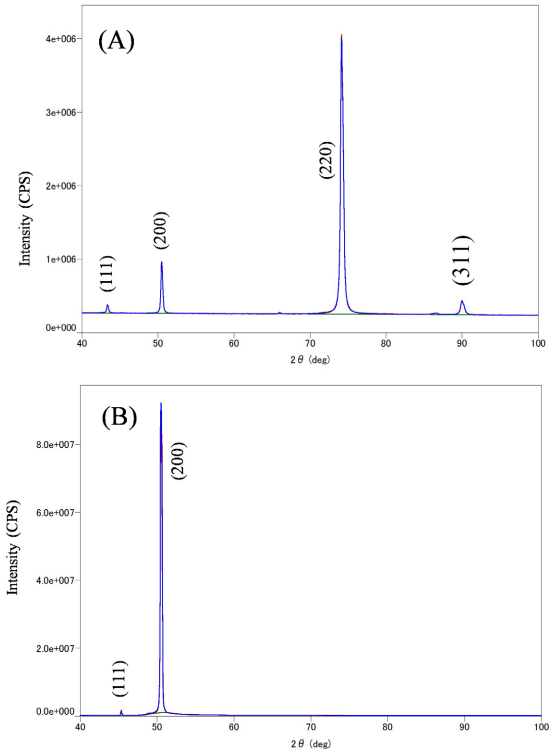

Figure 1. XRD patterns of Cu thin-film HA for (A) as-obtained and (B) after a vacuum heating at 473 K for 30 min.

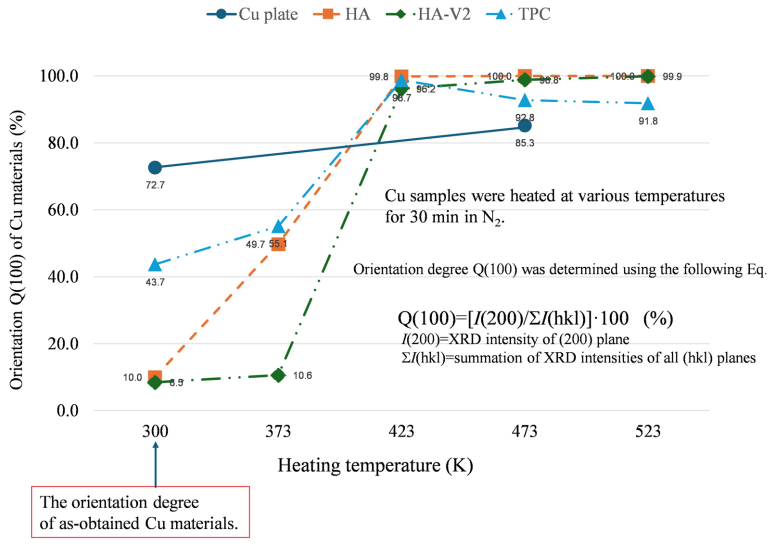

Figure 2. The orientation degrees Q(100) of Cu materials after heating.

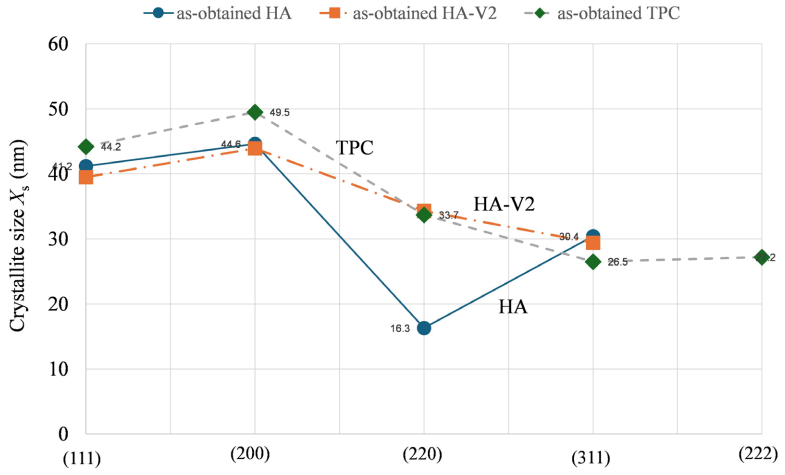

Figure 3. Crystallite sizes of each crystal plane of as-obtained Cu thin-films, HA, HA-V2 and TPC.

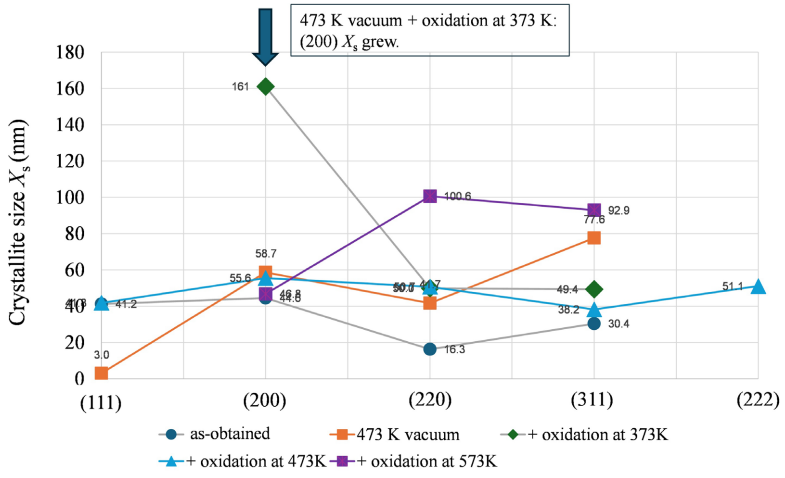

Figure 4. Crystallite sizes X_s at each crystal plane for heated Cu thin-films HA.

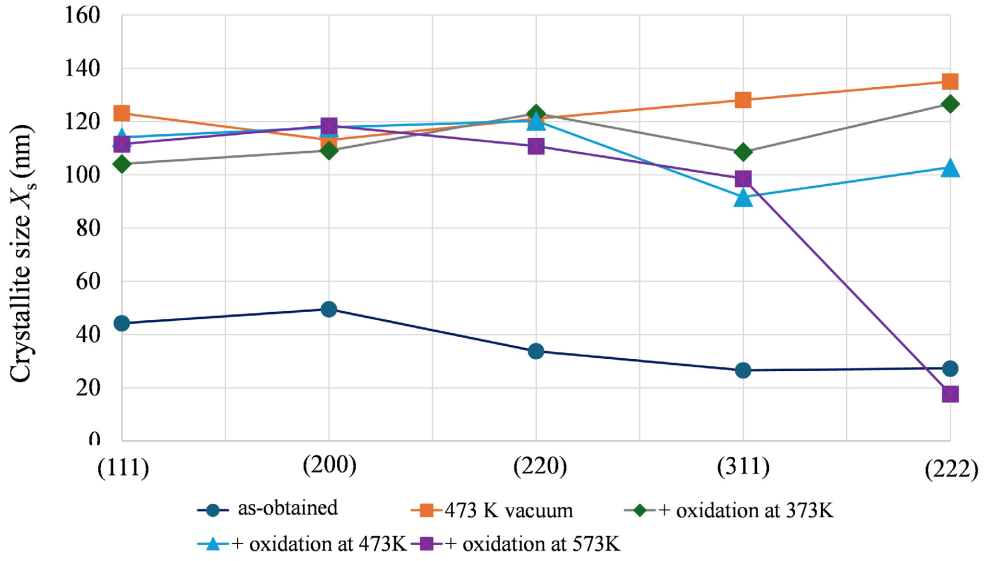

Figure 5. Crystallite sizes X_s at each crystal plane of heated Cu thin-films TPC. X_s of all planes are the same from 100 to 120 nm except for (222) plane.

3.2. Chemiluminescence of Cu Thin-Films Prepared under Various Conditions

Next, the chemiluminescence (CL) intensities of thin-films, which were heat-treated under various conditions, were measured for 9 min and summated. **Figure 6** summarized the results as simple overview, that is ΣCL (9 min) as a function of heating temperature; some intercalary vertical comments indicate the heating condition. Starting from the left hand, as-obtained thin-films revealing the ΣCL (9 min) values around 200 × 1000 counts (200 k·count), "473 K for 30 min in N_2" heated samples gave a small amount reduction, however, on the other hand, when a heating method was changed to "vacuum" ["473 K for 30 min in a vacuum"] ΣCL (9 min) increased to 512.6 (TPC), 701.8 (HA-V2), and 907.5 (HA) k·count. Between thin-films prepared in "N_2" and "vacuum" heating, crystallite sizes X_s and orientation degree Q(100) were the same. Therefore, much difference in ΣCL (9 min) values might come from the difference of outermost surface physicochemical condition; "vacuum" heating might bring the clean surface, on the other hand, "N_2" heating might not. Then, based on the idea that CL intensity, *i.e.* amount of reactive oxygen species ROS is generated on the Cu oxidative very thin films such as Cu_2O and CuO, two kinds of thin-film were re-oxidated at 373 K for 7 min in air after "vacuum" heating, this process could be considered to clean up the outermost surface once and reconstruct Cu-oxide thin-films. HA film showed the highest ΣCL (9 min) around 1600, followed by 775 (HA-V2) and 540 (TPC) k·count as shown in **Figure 6**. However, further re-oxidation at the higher temperatures resulted in the decrease of ΣCL (9 min). Therefore, the combination of the vacuum (473 K/30 min) and re-oxidation (373 K/7 min/air) was thought to be the optimum process to give the maximum ΣCL (9 min). Other HA-V2 and TPC thin-films also showed the best values in this combination process among them.

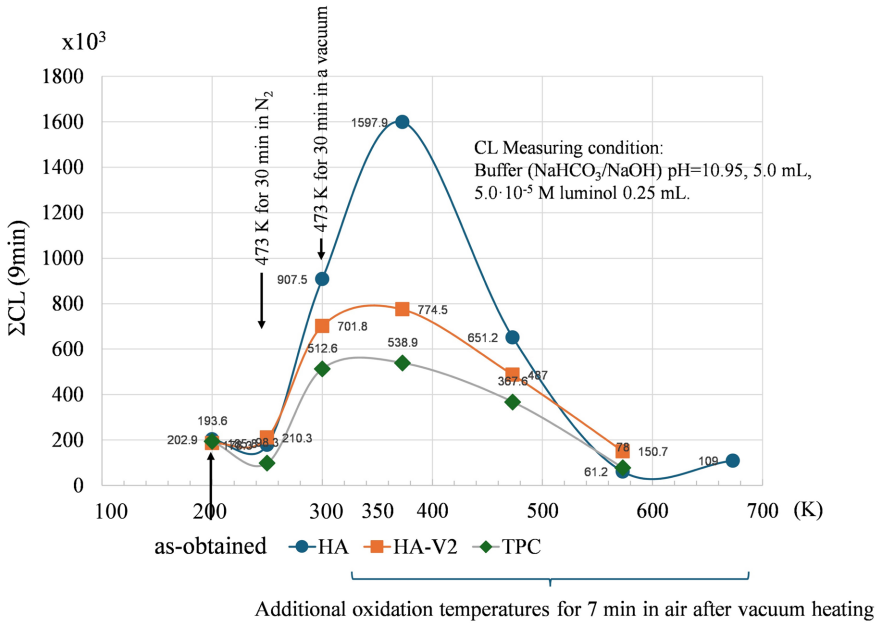

Figure 6. Summation CL of Cu thin-films prepared under various conditions.

3.3. Grain Orientations and ΣCL (9 min) of Cu Thin-Films

Figure 7 shows various grain orientation degrees, such as Q(110), Q(100) and Q(111), with the summation of CL intensity, Σ (CL) (9 min) of HA thin-film prepared under DP vacuum (2.0×10^{-3} Pa) at various temperatures for 1.8×10^3 s (30 min). The CL measurement conditions were the same as those mentioned before, such as buffer's pH: 10.7, 5.0 mL and 5.0×10^{-5} M luminol solution, 0.25 mL.

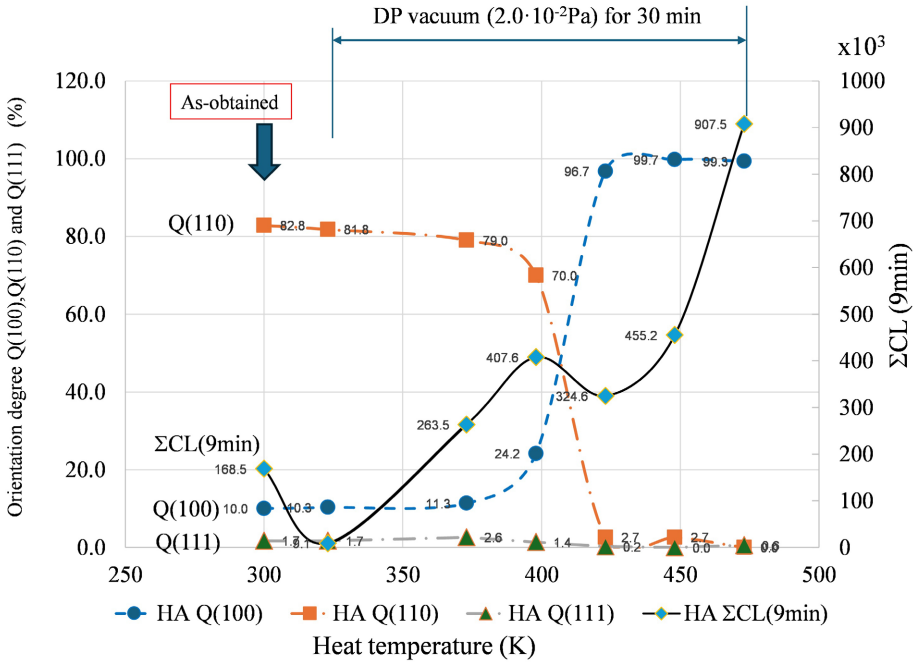

Figure 7. Various orientation degrees and ΣCL for HA thin-film treated under DP vacuum for 30 min.

It is safe to say that Σ (CL) (9 min) value depends much on Q(100). From 325 K to 400 K, Q(100) increased a little from 10.2 to 24.2% and on the contrary, Q(110) decreased a little from 82.8 to 70.0%. If we could presume that Q(100) and Q(110) have positive and negative effects on Σ (CL) (9 min), respectively, a little increment/decrement could bring a gradual increase of Σ (CL) (9 min). Furthermore, at temperatures around 400 to 425 K, with increasing Q(100), at the same time with decreasing Q(110), Σ (CL) (9 min) increased gradually, being independent on Q(111). At higher than about 425 K, nevertheless, the constant value of Q(100), Σ (CL) (9 min) increased rapidly. This might be explained by the grain growth of (100)-plane at these temperatures. As far as counter part of TPC thin-film is concerned, as shown in **Figure 8**, the same trend as HA with increasing Q(100) and decreasing Q(110) could be recognized. Therefore, it might be probably true that Σ (CL) (9 min) value depends much on Q(100).

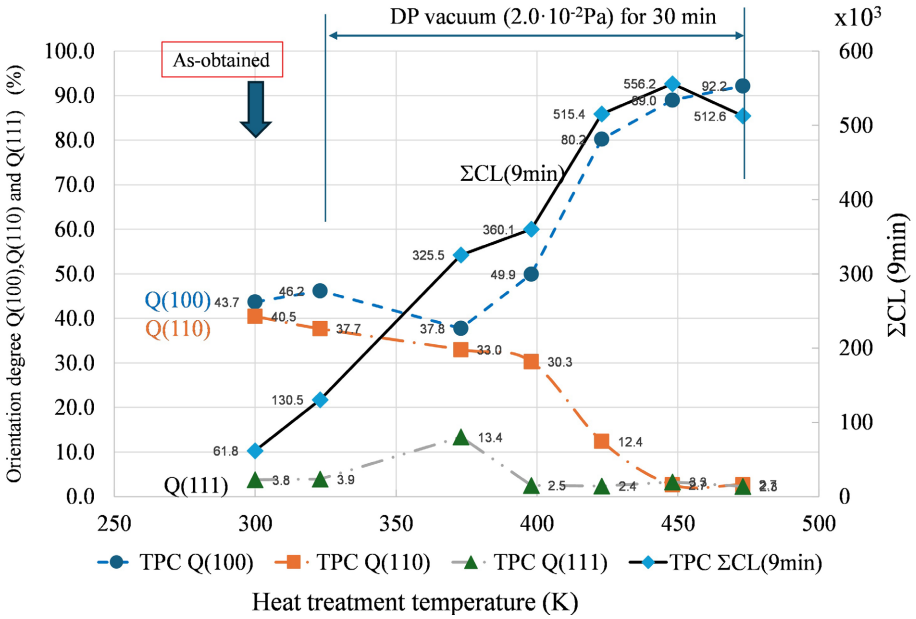

Figure 8. Various orientation degrees and ΣCL for TPC thin-film treated under DP vacuum for 30 min.

This phenomenon could be explained as follows:

1) It has been reported that the structure of Cu oxide thin-film is a stacked layer from bottom to top Cu/Cu_2O/CuO [6] [23] [24].

2) The growing rate of Cu oxide thin-film on Cu(100) plane is much higher than those of Cu(111) and Cu(110) [25]. Here, it should be noted that these results were pointed by Iijima [25] using Cu single crystal.

3) The high growing rate of Cu oxide films on Cu(100) might introduce easily some defects in thin-film, such as facets, steps, and/or kinks.

4) As shown in **Figure 9**, ROS may be produced at these defects at the Cu_2O/CuO thin-film layer formed on the outermost surface of Cu, because these defects are very active physically [26]. Generation of reactive oxygen species (ROS) around

above mentioned "steps", and/or "kink" in the Cu_2O/CuO thin-film layer was explained using chemical reaction equations shown in Figure 9.

As the amount of ROS reflects the Σ (CL) values, therefore, Cu(100) plane can give high Σ (CL). As mentioned, the high growing rate of Cu oxide thin-film, here, we consider Cu oxide thin-film could be Cu_2O, on Cu(100) could be explained qualitatively.

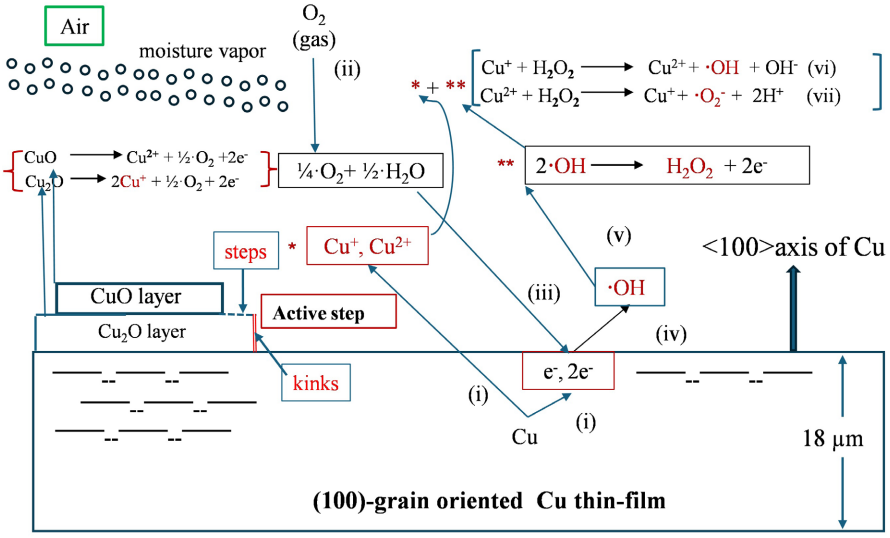

Figure 9. Schematic diagram for "Fenton reaction" to produce "ROS, ·OH, $\cdot O_2^-$" on the surface of Cu plate with thin copper oxides.

Figure 10 shows the crystal structure of (A) face-centered-cubic (FCC) Cu [27] and (B) simple cubic *Pn3m* Cu_2O (cuprite) [28]. Oxygen ions in Cu_2O occupy the eight corners of cubic cell and inside it, and four Cu^+ ions form a regular tetrahedron, *i.e.* Cu^+: (1/4, 1/4, 1/4), (1/4, 3/4, 3/4), (3/4, 1/4, 3/4), (3/4, 3/4, 1/4) [29]: O_2^-: (0, 0, 0), (1/2, 1/2, 1/2). It should be noted that Cu_2O unit cell contains a regular tetrahedron of Cu_4O.

If the outermost surface of Cu is oxidized, it can be questioned which crystal plane is suitable for the first formation of Cu_2O. Figure 10 also shows a schematic configuration of regular tetrahedron of Cu_4O positioned on (i) (100), (ii) (110), and (iii) (111) planes of Cu; large brown circles in each plane are Cu atoms (atomic radius = 0.128 nm) [30], and small brown and large broken-line circles of regular tetrahedron Cu_4O present Cu^+ (ionic radius with the coordination number 2, 0.046 nm) [31] and O_2^- (ionic radius with the coordination number 4, 0.138 nm) [31] ions, respectively. In addition, the diagonal length of regular tetrahedron $I_{Cu\text{-}Cu(Cu2O)}$ is $2^{-1/2}\cdot a_{(Cu2O)}$ = 0.30066 nm and the side length of square (100) is $a_{(Cu)}$ = 0.35819 nm. Here, the lattice parameters $a_{(Cu)}$ = 0.35819 nm (PDF#4105040) and $a_{(Cu2O)}$ = 0.42520 nm (PDF#1000063) were used for calculation. Here, it should be noticed that the density of Cu-Cu pair ("red star symbol") with the shortest distance per unit area, *Den*(Cu-Cu); (i) *Den*(Cu-Cu) on Cu(100) plane: $4/a_{(Cu)}^2$, (ii) *Den*(Cu-Cu) on Cu(110) plane: $2^{1/2}/a_{(Cu)}^2$, (iii) *Den*(Cu-Cu) on Cu(111) plane:

$3^{1/2}/a_{(Cu)}^2$. Therefore, *Den*(Cu-Cu) for C(100) is the highest and followed by those of Cu(111) and Cu(110) planes. This order agrees well with the growth rate of Cu oxide thin-films on Cu planes. Furthermore, Cu atom in the center of Cu(100) plane might have some influence on making Cu-O bonding at first. Based on these configurations and relaxed structure metal surface of Cu, we presumed that Cu(100) plane might provide better stable situation for the formation of thin-film of Cu_2O readily than others.

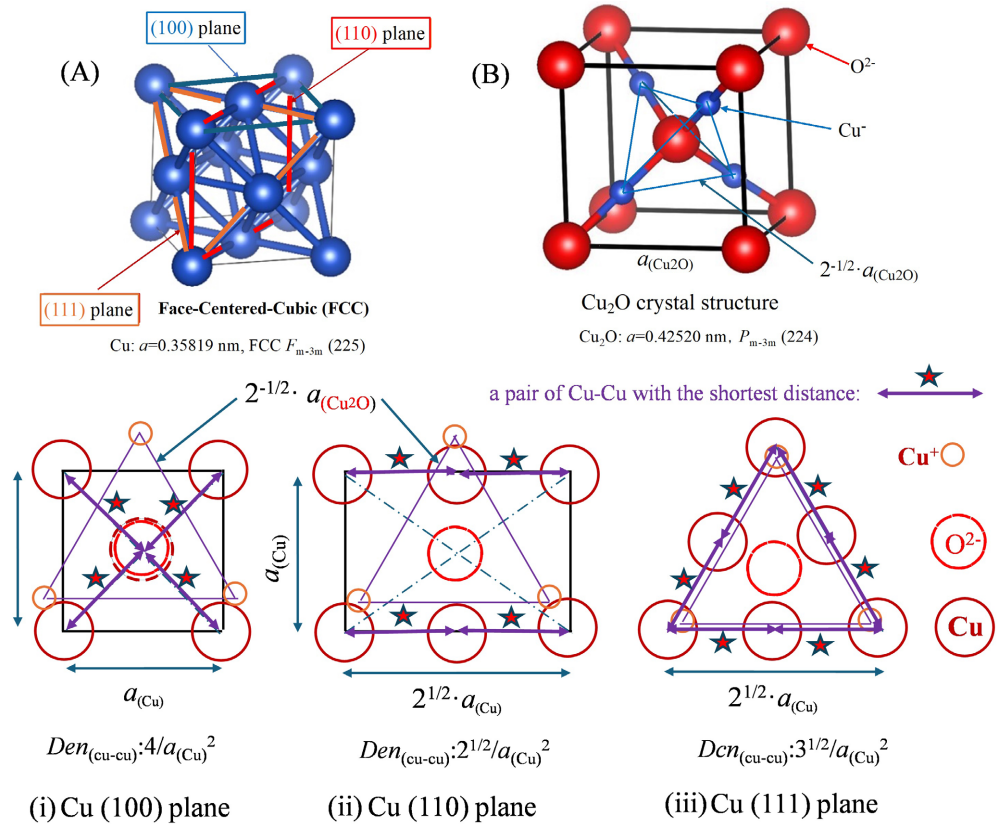

Figure 10. Schematic diagram for the configuration of regular tetrahedron of Cu_4O on: (i) (100), (ii) (110) and (iii) (111) planes of FCC Cu. Purple circle present Cu: large one of each plane, and small one of regular tetrahedron of Cu_2O, and red large circle O of regular tetrahedron of Cu_2O.

3.4. SEM and TEM Observation on Cu Thin-Films Prepared under Various Conditions

Then, the microstructure of most upper (outermost) surface of HA was observed using SEM and TEM. **Figure 11** shows the micrographs of thin films, No. 1 is as-obtained HA with the Σ (CL) (9 min) = 111.6 k·count, No. 2 after heating at 473 K for $1.8 \cdot 10^3$ s (30 min) in N_2 the with Σ (CL) (9 min) = 396.3 k·count, No. 3 after vacuum heating (DP) at 473 K for 30 min with the Σ (CL) (9 min) = 907.5 k·count, and No. 4 after vacuum heating (DP) and re-oxidation at 373 K for 7 min in air with the Σ (CL) (9 min) = 1597.9 k·count. At a glance, the surface of No. 2 is different from others, *i.e.* consisting of granularity, and others are cloudlike textures. Then, the most upper surfaces of No. 2 and No. 4 samples were observed

using TEM. Figure 12 shows the cross-section of outermost surface of No. 2, indicating the line-analysis position and intensities of Cu/Pt, respectively. By comparing (A) and (B), it is clear that black and grey regions on (A) are Cu and Cu_2O_{1-x}, and black bulk in right side is Pt passivating film. And it is characteristic that a few accentuated cylinders consisting of Cu_2O_{1-x} covered with a hat-like Pt are formed on the Cu base. In Figure 12(C), atomic intensities are presented as bar graph. Figure 13 shows TEM images and elemental analysis for the outermost surface of No. 4 heated at 473 K for 1.8×10^3 s (30 min) in a vacuum, followed by heating 373 K for 7 min in air (re-oxidation); (A) is the cross-section image with a horizontal line indicating point-analysis position, (B) and (C) are elemental-analysis bar graph and atomic density on each position, respectively. It should be noted that in Figure 13, no accentuated cylinders are recognized and only two kinds of thin layers are observed. From the position number on the blue line in (A) and each point analysis data shown as bar graph in (B), numbers from "1" to "3" represent mainly Cu base, and "4" and "5" suggest Cu_2O_{1-x} and CuO, respectively. This change in composition corresponds to the color change of image shown in (A). Here, we should pay attention that the CL summation ΣCL of the latter of No. 4 (vacuum and re-oxidized) is much higher than that of former sample No. 2 (N_2 heating) in Figure 11. That is, the outermost surface, which consists of graded double thin layers of Cu_2O_{1-x} and CuO could produce more ROS than that of the accentuated cylinders consisting of Cu_2O_{1-x}.

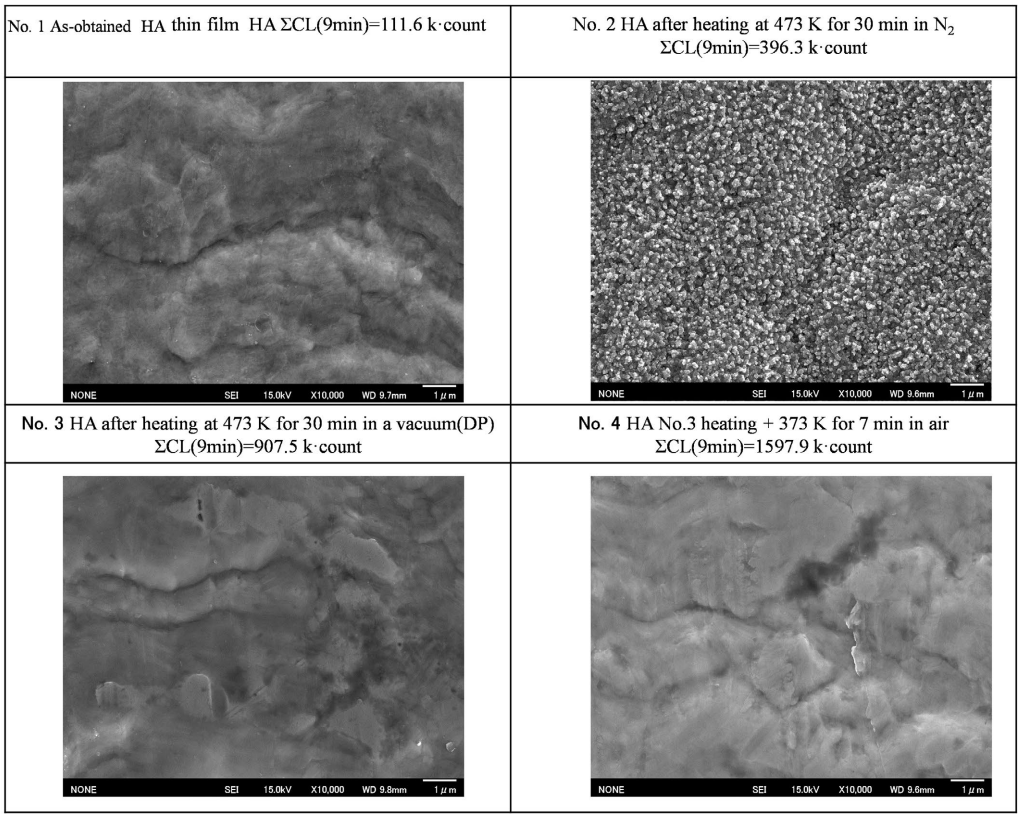

Figure 11. SEM images of the surfaces of Cu thin-films after various heat treatments.

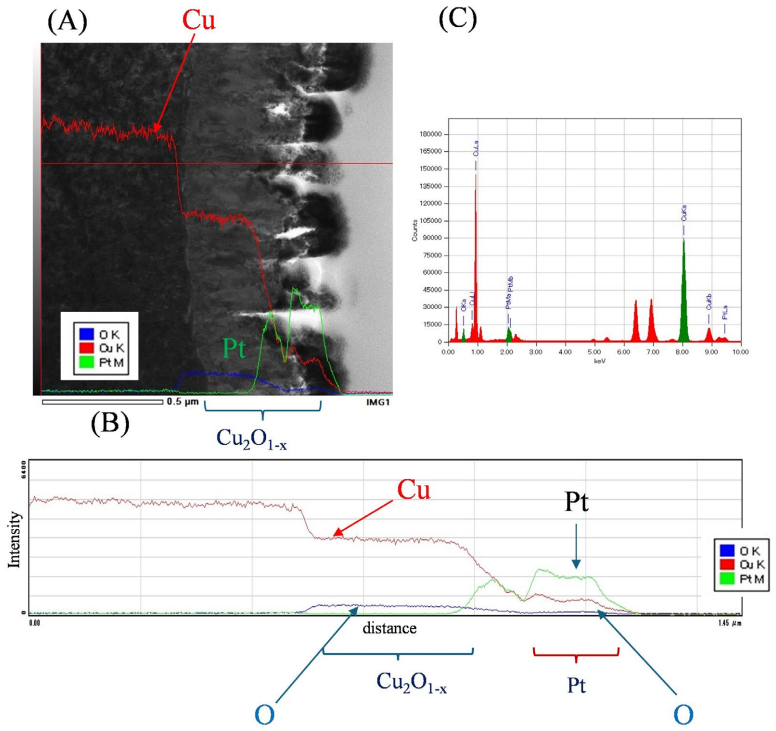

Figure 12. TEM images and elemental analysis for the outermost surface of HA after heating at 473 K for 30 min in N_2; (A) is the cross-section images with a horizontal red line indicating line-analysis position, (B) and (C) are elemental intensity distribution and bar graph, respectively.

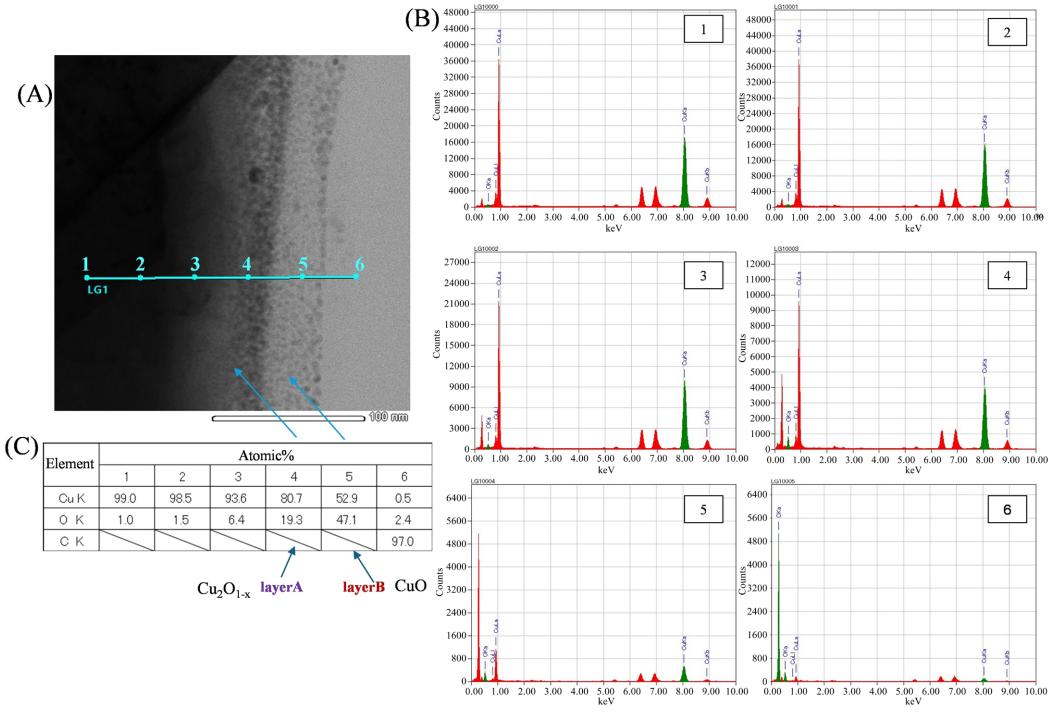

Element	Atomic%					
	1	2	3	4	5	6
Cu K	99.0	98.5	93.6	80.7	52.9	0.5
O K	1.0	1.5	6.4	19.3	47.1	2.4
C K						97.0

Figure 13. TEM images and elemental analysis for the outermost surface of No. 4 heated at 473 K for 30 min in a vacuum, followed by heating 373 K for 7 min in air (reoxidation); (A) is the cross-section image with a horizontal vlue line indicating point-analysis position, (B) and (C) are elemental analysis bar graph and atomic density on each position, respectively.

3.5. ROS Generated on Cu Thin-Films Prepared under Various Conditions

Then, it was investigated which ROS was produced on the outermost surface using corresponding scavengers during CL measurement, as shown in Table 1. In order to determine the most optimum additive amount of each scavenger, ΣCL for Cu thin film HA, which was heated under vacuum and then re-oxidized at 373 K/7min in air was measured. Figure 14 presents their results; as the most optimum additive amount could give the minimum ΣCL, the optimum additive amounts for scavenger of 2-propanol ("2-pro") for ·OH, sodium pyruvate ("s-pyr") for H_2O_2, nitro blue tetrazolium ("nbt") for $\cdot O_2^-$ were 5.0×10^{-5} M with 0.5 mL. However, the optimum amount for sodium azide ("NaN_3"), for $^1O_2$ was 5.0×10^{-5} M with 1.0 mL under the conditions of 5.0×10^{-5} M luminol 0.25 mL.

Table 1. Comparison of ROS components for thin-film HA and Cu plate.

	HA		Cu plate	
	as-received	DP + 373 K (7 min/air)	as-received	373 K (7 min/air)
·OH	28.93	21.47	25.8	20.6
H_2O_2	20.83	21.41	35.00	44.7
$\cdot O_2^-$	20.64	25.51	38.1	24.9
$^1O_2$	29.60	31.61	1.00	10.40
ΣCL (9min) (k·count)	**125**	**1281**	111.6	254.1

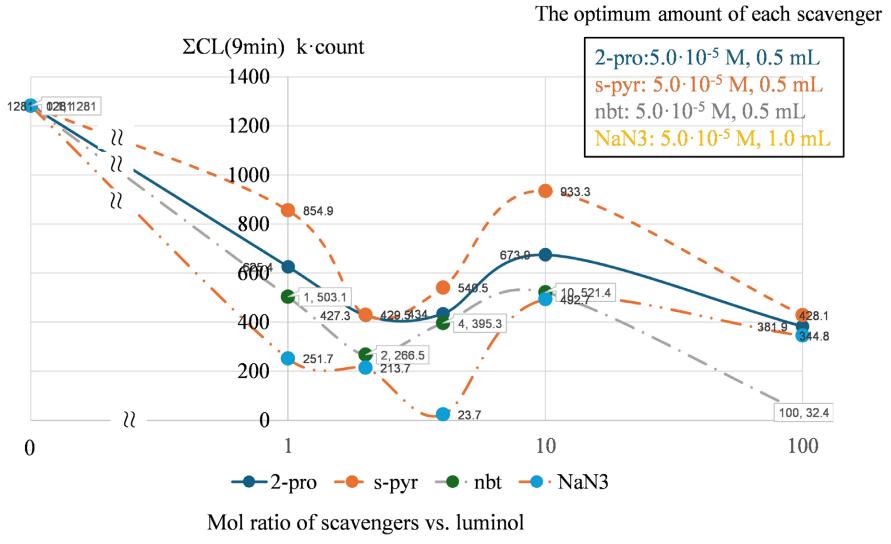

Figure 14. Scavenger effect on the summation of CL intensity for vacuum + 373 K/7 min/air treated Cu thin-film HA.

Figure 15 shows the component of ROS generated on the surface of Cu plate prepared under various conditions. It is interesting that "DP" (vacuum heating at 473 K for 1.8×10^3 s (30 min)) treatment brings ever-increasing ROS, such as, ·OH <

$H_2O_2 < O_2^- < {}^1O_2$. However, once after oxidizing, ·OH and H_2O_2 were recovered. On the contrary, as shown in Figure 16, it is extreme that H_2O_2 and O_2^- have disappeared from HA thin-film after DP. As the same as Cu plate, once after oxidizing, all ROS have been generated again. These phenomena can suggest that: 1) DP treatment can bring passive oxidation [32] to both Cu outermost surfaces, and 2) its effect is stronger on HA thin-film than conventional Cu plate, it might be due to the hard/severe processing condition to fabricate thinner films from the thicker sheet.

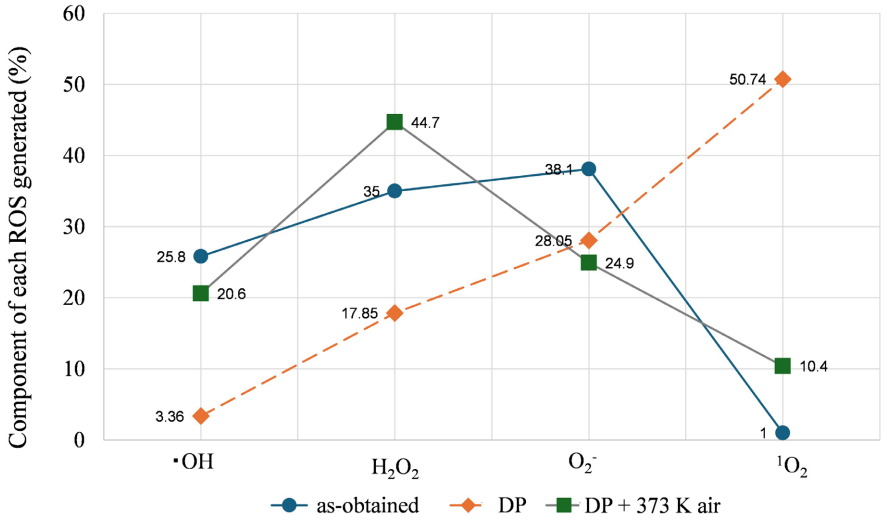

Figure 15. Comparison of ROS generated on the Cu plates prepared under various heating conditions.

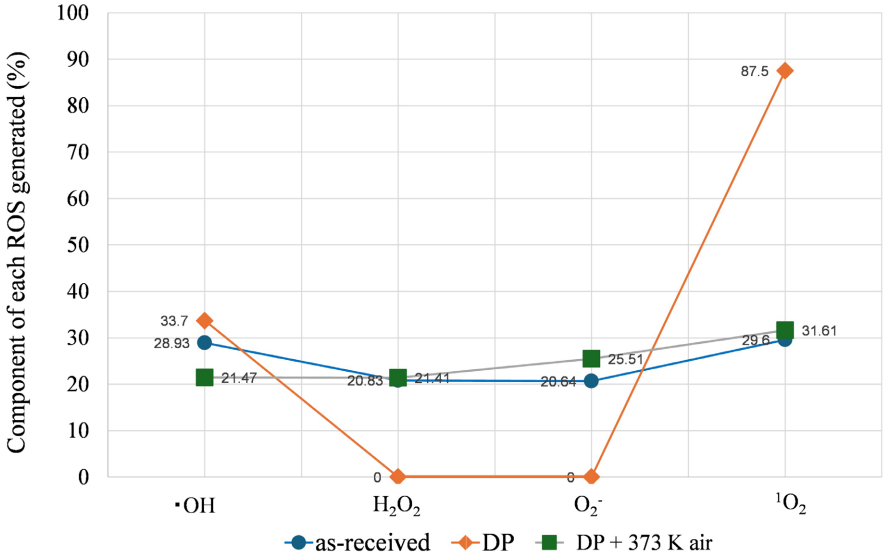

Figure 16. Comparison of ROS generated on the Cu thin-film HA prepared under various heating conditions.

3.6. Re-Oxidation Conditions for Cu Thin-Films

For further study, the optimum vacuum heating and re-oxidation conditions were

investigated. Figure 17 shows ΣCL of the Cu thin-film HA after vacuum heating (at 473 K for 1.8×10^3 s (30 min)), followed by re-oxidation for 0 - 60 min at 373 and 398 K in air. ΣCL values plotted with ultramarine blue circles are those of HA re-oxidized at 373 K and other shapes such as triangle (back), square (top) and red circles (top) present are those of HA re-oxidized at 398 K for 1.8×10^3 s (30 min). Here, "top" or "bottom" means that HA films were stacked in top and bottom in layers during re-oxidation. The latter three kinds of shape indicate the dispersion of measured values. From this graph, it might be concluded that the best ΣCL was achieved for HA thin-film heated under vacuum and re-oxidized at 398 K for 1.8×10^3 s (30 min) in air.

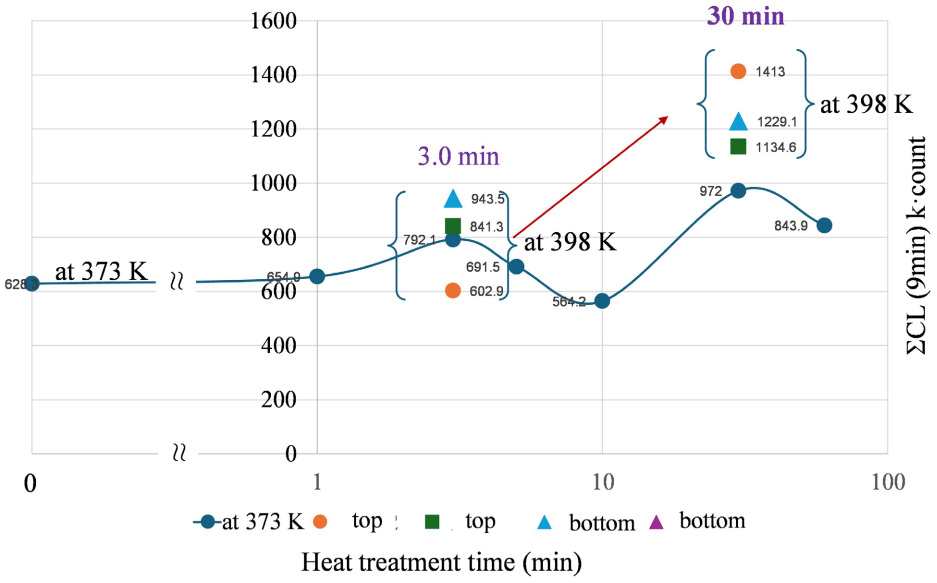

Figure 17. ΣCL of the Cu thin-film HA after vacuum heating, followed by reoxidation for 0 - 60 min at 373 and 398 K in air.

3.7. Biotest of Cu Thin-Films

As stated previously, antibacterial activity value *R* (*a-a-R*) of: 1) as-obtained and 2) antibacterial activity improved HA films were evaluated. Figure 18 shows their (*a-a-R*) vs. lapse time: evaluated for 8.64×10^4 s (24 h) and 1.8×10^3 s (30 min) at 393 K using *Escherichia coli* (*E. coli*), *Staphylococcus aureus* (*S. aureus*) and *A/Hong Kong virus*. After long lapse time 8.64×10^4 s (24 h), there is little difference between improved HA and as-obtained thin films in (*a-a-R*) against *E. coli*, *S. aureus* and *A/Hong Kong virus*. It is clear that these bacteria and viruses are strong in this order. However, at shorter lapse time of 1.8×10^3 s (30 min), it should be noted that: 1) (*a-a-R*) of the former (3.6) is a little higher than that of the latter (2.6) against for *E. coli*, and 2) scattering of (*a-a-R*), *i.e.* the length of vertical arow, of the former is small in comparison with that of the latter against for both *E. coli* and *S. aureus*. This means that at long lapse time of 8.64×10^4 s (24 h) required lapse time by JIS (Japan Industrial Standard), the former HA showed the almost same antibacterial activity as the commercially available HA; little

improvement was recognized. However, at shorter lapse time, the former overcomes the latter in a viewpoint of (*a-a-R*), and a small scattering (that is antibacterial activity level is stable).

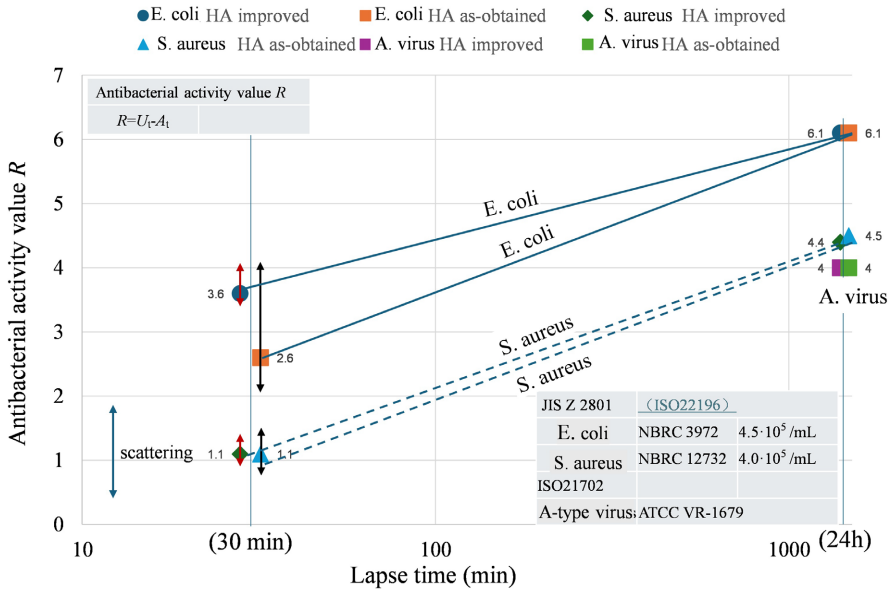

Figure 18. Antibacterial activity values *R* for Cu thin-films of both as-obtained and antibacterial activity improved, evaluated for 24 h and 30 min at 393 K using Escherichia coli (*E. coli*), Staphylococcus aureus (*S. aureus*) and *A/Hong Kong virus*.

4. Conclusion

By focusing on generation of reactive oxygen species (ROS) on the copper surface, the antibacterial activity of copper has been tried to explain. Especially, the change in ROS formed on the heated Cu plate was investigated: hydroxyl radical ·OH, hydrogen per oxide H_2O_2, and superoxide anion $\cdot O_2^-\cdot$ are the most of ROS. These data concerning the components of ROS formed on the surface of heated Cu are reported for the first time using chemiluminescence with the combination of luminol and scavengers. In addition, the generation mechanism of these three ROS on the outermost surface consisting of thin film Cu_2O, CuO layer and bulk Cu is also proposed. If the strong antibacterial activity is required in the industrial markets, such as aircrafts, automobiles and marine vessels, a lot of (100) plane-oriented Cu thin-film will be adopted. The enhancement of disinfect mechanism on Cu (100) plane and the composition of ROS will be elucidated in the future.

Acknowledgements

The authors thank Ms. M. Toda of the Doshisha University Research Centre for Interfacial Phenomena for FE-SEM and TEM observations of the samples.

Conflicts of Interest

The authors declare no conflicts of interest regarding the publication of this paper.

References

[1] Hirota, K., Tanaka, H., Maeda, T., Tsukagoshi, K., Kawakami, H., Ozawa, T., *et al.* (2023) Evaluation of Reactive Oxygen Species (ROS) Generated on the Surface of Copper Using Chemiluminesence. *Materials Sciences and Applications*, **14**, 482-499. https://doi.org/10.4236/msa.2023.1410032

[2] Vincent, M. Duval, R.E., Hartemann, P. and Engels-Deutsch, M. (2018) Contact Killing and Antimicrobial Properties of Copper. *Journal of Applied Microbiology*, **124**, 1032-1046. https://doi.org/10.1111/jam.13681

[3] Govind, V., Bharadwaj, S., Sai Ganesh, M.R., Vishnu, J., Shankar, K.V., Shankar, B., *et al.* (2021) Antiviral Properties of Copper and Its Alloys to Inactivate Covid-19 Virus: A Review. *BioMetals*, **34**, 1217-1235. https://doi.org/10.1007/s10534-021-00339-4

[4] Grass, G., Rensing, C. and Solioz, M. (2011) Metallic Copper as an Antimicrobial Surface. *Applied and Environmental Microbiology*, **77**, 1541-1547. https://doi.org/10.1128/aem.02766-10

[5] Salah, I., Parkin, I.P. and Allan, E. (2021) Copper as an Antimicrobial Agent: Recent Advances. *RSC Advances*, **11**, 18179-18186. https://doi.org/10.1039/d1ra02149d

[6] Honkanen, M., Vippola, M. and Lepistö, T. (2008) Oxidation of Copper Alloys Studied by Analytical Transmission Electron Microscopy Cross-Sectional Specimens. *Journal of Materials Research*, **23**, 1350-1357. https://doi.org/10.1557/jmr.2008.0160

[7] Onu, A.D., Iyun, J.F. and Idris, O.S. (2015) Kinetics and Stoichiometry of the Reduction of Hydrogen Peroxide by an Aminocarboxylactocobaltate(II) Complex in Aqueous Medium. *Open Journal of Inorganic Chemistry*, **5**, 75-82. https://doi.org/10.4236/ojic.2015.54009

[8] Chambers, S.A. (2000) Epitaxial Growth and Properties of Thin Film Oxides. *Surface Science Reports*, **39**, 105-180. https://doi.org/10.1016/s0167-5729(00)00005-4

[9] Yu, Z., Ramdani, J., Curless, J.A., Overgaard, C.D., Finder, J.M., Droopad, R., *et al.* (2000) Epitaxial Oxide Thin Films on Si (001). *Journal of Vacuum Science & Technology B: Microelectronics and Nanometer Structures Processing, Measurement, and Phenomena*, **18**, 2139-2145. https://doi.org/10.1116/1.1303737

[10] Hilleringmann, U. (2023) Silicon Semiconductor Technology: Processing and Integration of Microelectronic Devices. English Edition, Springer Vieweg.

[11] JX Home Page (2024) "Rolled Copper Foil" of JX Advanced Metal Corporation in Japanese. https://www.jx-nmm.com/products/

[12] Zhang, Y., Dai, M. and Yuan, Z. (2018) Methods for the Detection of Reactive Oxygen Species. *Analytical Methods*, **10**, 4625-4638. https://doi.org/10.1039/c8ay01339j

[13] Reitberger, T. and Gierer, J. (1988) Chemiluminescence as a Means to Study the Role of Hydroxyl Radicals in Oxidative Processes. *Holzforschung*, **42**, 351-356. https://doi.org/10.1515/hfsg.1988.42.6.351

[14] Tsukagoshi, K., Sumiyama, M., Nakajima, R., Nakayama, M. and Maeda, M. (1998) Chemiluminescence Property of the Luminol-Hydrogen Peroxide-Copper (II) System in the Presence of Surface-Carboxylated Microspheres. *Analytical Sciences*, **14**, 409-412. https://doi.org/10.2116/analsci.14.409

[15] Yu, W. and Zhao, L. (2021) Chemiluminescence Detection of Reactive Oxygen Species Generation and Potential Environmental Applications. *TrAC Trends in Analytical Chemistry*, **136**, Article ID: 116197. https://doi.org/10.1016/j.trac.2021.116197

[16] Oba, S. and Mukai, T. (2010) Mechanism and Condition of the Chemiluminescence of Luminol and Lucigenin. *Keio University, Hiyoshi Review of Natural Science*, **48**, 31-57.

[17] ThermoFisher Scientific Home Page (2024) Home Technical Reference Library the Molecular Probes Handbook List of Tables Scavengers of Reactive Oxygen Species (ROS)—Table 18.2. https://www.thermofisher.com/

[18] Greenwald, R.A. (1985) CRC Handbook of Methods for Oxygen Radical Research. CRC Press.

[19] Billany, M.R., Khatib, K., Gordon, M. and Sugden, J.K. (1996) Alcohols and Ethanolamines as Hydroxyl Radical Scavengers. *International Journal of Pharmaceutics*, **137**, 143-147. https://doi.org/10.1016/0378-5173(96)04246-9

[20] Wang, L., Li, B., Dionysiou, D.D., Chen, B., Yang, J. and Li, J. (2022) Overlooked Formation of H_2O_2 during the Hydroxyl Radical-Scavenging Process When Using Alcohols as Scavengers. *Environmental Science & Technology*, **56**, 3386-3396. https://doi.org/10.1021/acs.est.1c03796

[21] Nishibori, S. and Namiki, K. (1998) Superoxide Anion Radical-Scavenging Ability of Fresh and Heated Vegetable Juices. *Nippon Shokuhin Kagaku Kogaku Kaishi*, **45**, 144-148. https://doi.org/10.3136/nskkk.45.144

[22] Vinila, V.S. and Isac, J. (2022) Synthesis and Structural Studies of Superconducting Perovskite $GdBa_2Ca_3Cu_4O_{10.5+\delta}$ Nanosystems. In: *Design, Fabrication, and Characterization of Multifunctional Nanomaterials*, Elsevier, 319-341. https://doi.org/10.1016/b978-0-12-820558-7.00022-4

[23] Zhu, Y., Mimura, K. and Isshiki, M. (2002) Oxidation Mechanism of Copper at 623-1073 K. *Materials Transactions*, **43**, 2173-2176. https://doi.org/10.2320/matertrans.43.2173

[24] Wang, J. and Cho, W.D. (2009) Oxidation Behavior of Pure Copper in Oxygen and/or Water Vapor at Intermediate Temperature. *ISIJ International*, **49**, 1926-1931. https://doi.org/10.2355/isijinternational.49.1926

[25] Iijima, J. (2005) Oxidation Behaviour of Copper at Low Temperatures. Ph.D. Thesis, Tohoku University.

[26] Homma, T. (1968) Microscopic Studies on the Oxidation Mechanism of Metal—A Role of Crystal Lattice Imperfection. *Journal of Institute of Industrial Science, The University of Tokyo*, **20**, 349-353.

[27] Jona, F. and Marcus, P.M. (2001) Structural Properties of Copper. *Physical Review B*, **63**, Article ID: 094113. https://doi.org/10.1103/physrevb.63.094113

[28] Ito, T., Yamaguchi, H., Okabe, K. and Masumi, T. (1998) Single-Crystal Growth and Characterization of Cu_2O and CuO. *Journal of Materials Science*, **33**, 3555-3566. https://doi.org/10.1023/a:1004690809547

[29] Galaso, F.S. (1975) Structure and Properties of Inorganic Solids. Pergamon Press.

[30] Atomicradius. https://en.wikipedia.org/wiki/atomicradius

[31] Shannon, R.D. (1976) Revised Effective Ionic Radii and Systematic Studies of Interatomic Distances in Halides and Chalcogenides. *Acta Crystallographica Section A*, **32**, 751-767. https://doi.org/10.1107/s0567739476001551

[32] Narushima, T., Goto, T., Hirai, T. and Iguchi, Y. (1997) High-Temperature Oxidation of Silicon Carbide and Silicon Nitride. *Materials Transactions, JIM*, **38**, 821-835. https://doi.org/10.2320/matertrans1989.38.821